Journal of Applied Fluid Mechanics, Vol. 18, No. 10, pp. 2476-2487, 2025.
Available online at www.jafmonline.net, ISSN 1735-3572, EISSN 1735-3645.
https://doi.org/10.47176/jafm.18.10.3480

Optimization Study of Centrifugal Fan Volute Parameters based on Non-dominated Sorting Genetic Algorithm III Algorithm

J. L. Li [1, 2], X. J. Wang[1, 2†], H. Gong[3], and J. J. Wang[1, 2]

[1] *Faculty of Mechanical and Electrical Engineering, Kunming University of Science and Technology, Kunming, Yunnan, 650500, China*
[2] *Yunnan Provincial Key Laboratory of Advanced Equipment Intelligent Manufacturing Technology, Kunming, Yunnan, 650500, China*
[3] *Engineering Training Center, Kunming University of Science and Technology, Kunming, Yunnan, 650500, China*

†*Corresponding Author Email: km_wxj@kust.edu.cn*

ABSTRACT

To enhance the operational effectiveness of centrifugal fans under specific operating conditions, a Backpropagation (BP) neural network, combined with a reference point-based Non-dominated Sorting Genetic Algorithm III (NSGA-III), numerical simulation, and other techniques, was employed to perform multi-objective optimization. Three structural parameters of the fan volute, volute height (h), the minimum distance between the impeller and the volute tongue (β), and the radius of the volute tongue corner (r), were selected as design variables. Two performance indicators, outlet flow rate (Q) and total pressure efficiency (η), were chosen as optimization objectives. An efficient and accurate BP neural network was established as a surrogate model for predicting volute performance, and optimal design parameter combinations were obtained using the NSGA-III algorithm. The optimization results were subsequently validated through both experimental and numerical simulations. The results demonstrated strong agreement between simulation and experimental data. The BP neural network provided highly accurate fitting and predictions, yielding a reliable surrogate model. After optimization, the centrifugal fan's Q increased by 2.29%, and η improved by 2.96%. Furthermore, structural improvements at the fan inlet enhanced the overall flow field, leading to a 6.06% increase in Q and a 4.04% increase in η compared to the original design. Overall, the dual optimization objectives were significantly improved, successfully meeting the specific operational requirements.

Article History

Received March 4, 2025
Revised April 19, 2025
Accepted May 15, 2025
Available online August 5, 2025

Keywords:

Centrifugal fan
Multi-objective optimization
Numerical simulation
BP-neural network
Non-dominated sorting genetic algorithm III

1. INTRODUCTION

Centrifugal fans are widely used in industrial applications, particularly for ventilation, dust removal and purification, and gas transport. However, they often encounter challenges such as insufficient airflow, low efficiency, and high energy consumption. This study focuses on optimizing the performance and design parameters of a centrifugal fan used by an enterprise in semiconductor production equipment for gas transfer. While the impeller is a standard, commercially purchased component, the volute and inlet/outlet ducts are independently designed. As a critical part of the production equipment, the fan circulates the cooled working medium within the system. The fan's operational setup is illustrated in Fig. 1, with a working pressure of 0.8 MPa, a temperature of 40°C, and nitrogen as the working medium. Under current operating conditions, the primary performance evaluation indicators are the outlet flow rate (Q) and the total pressure efficiency (η), with Q having a direct impact on semiconductor processing quality.

As the core components of a centrifugal fan, the volute and impeller significantly influence overall performance. Consequently, current optimization efforts for centrifugal fans primarily target these two elements. The impeller, as the only working component, has been extensively studied. Numerous researchers have demonstrated that design parameters such as the number of blades and mounting angle are strongly correlated with the aerodynamic performance of centrifugal fans (Shinbara et al., 1996; Wu et al., 2002; Ai & Chen, 2016; Tantakitti et al., 2018). Adjusting these parameters can

NOMENCLATURE

Q	outlet flow rate	L	outlet length
η	total pressure efficiency	H	total pressure
Z	number of impeller blades	H_{in}	inlet total pressure
h	volute height	H_{out}	outlet total pressure
β	minimum distance between the impeller and volute tongue	T	impeller shaft torque
r	radius of the volute tongue corner	ρ	density of the working medium
θ	outlet expansion angle	ω	fan rotational speed
E	extension length		

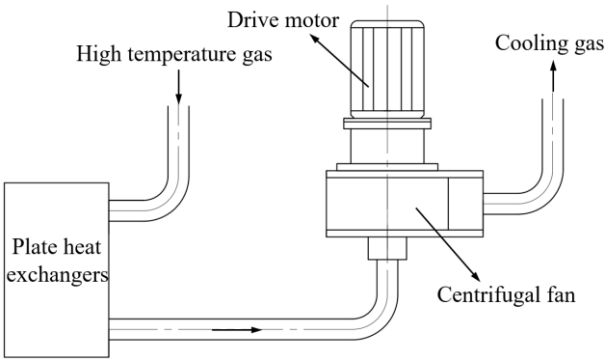

Fig. 1 Scenario diagram of fan operation

reduce vortex formation during impeller rotation, lower flow losses, and enhance performance.

During operation, the volute plays a critical role in collecting airflow, increasing pressure, and guiding the flow direction. Both domestic and international studies on volute optimization have mainly focused on how geometric parameters, such as the volute tongue's position, angle, and size, affect the outlet flow field (Zhao et al., 2012; Zhou et al., 2021). These efforts aim to prevent vortex formation at the outlet, which could otherwise induce secondary flow recirculation. Various methods, including the Levenberg-Marquardt algorithm and spiral angle adjustments, have been employed to refine volute contour design (Amiet, 1976; Li et al., 2012; Huang & Tseng, 2016; Zhou et al., 2018), improving outlet velocity uniformity and internal flow field smoothness, thereby enhancing fan performance. Additionally, parameters such as the vertical distance between the volute and impeller, the β, and other mutual positional relationships also affect turbulence near the volute tongue (Patil et al., 2018; Chen et al., 2019; Zhang et al., 2023), which in turn impacts fan performance and internal flow dynamics.

In multi-objective optimization of centrifugal fans, as the number of design variables and performance objectives increases, intelligent algorithms have gained widespread adoption. Techniques such as genetic algorithms (Zuo et al., 2016), particle swarm optimization (Wang et al., 2019), and artificial immune algorithms (Liang et al., 2023) have yielded promising results. To better model the nonlinear relationships between design parameters and performance indicators, surrogate models are frequently employed. Common approaches include artificial neural networks, Kriging models, and response surface methods (Liang et al., 2023). Among these, artificial neural networks have proven to be more suitable for complex nonlinear problems due to their superior accuracy, predictive efficiency, and stability (Li & Zheng, 2017). Furthermore, optimization and design methods proposed for aero-engine systems (Ma et al., 2024; Tao et al., 2024; Zhang et al., 2025) offer valuable reference points and inspire improvements in overall system performance.

In this study, the impeller is a standard off-the-shelf component, while the volute is independently designed by the company. To reduce optimization costs and accommodate specific operating conditions, this research focuses exclusively on the volute's optimization. Given the limited application of intelligent optimization algorithms to volute design alone, and considering the NSGA-III algorithm's advantages in maintaining diversity and utilizing reference point mechanisms for complex multi-objective problems, the volute design parameters are optimized using the NSGA-III algorithm. The optimization objectives are the fan's Q and η. The Plackett–Burman method is applied for significance analysis, identifying three key design variables: volute height (h), the minimum distance between the impeller and the volute tongue (β), and the radius of the volute tongue corner (r). Using the Latin Hypercube Sampling method, 50 sets of structural parameters are generated. Numerical simulations of a non-simplified model are then conducted in FLUENT to obtain target values, forming the sample dataset. A high-precision BP neural network is trained as a surrogate model using this dataset. Finally, the NSGA-III algorithm is used to determine the optimal structural parameters corresponding to the desired performance objectives.

2. MODELING AND NUMERICAL SIMULATION

2.1 Centrifugal Fan Model Establishment and Mesh Generation

The subject of this study is a forward-curved multi-blade centrifugal fan independently designed by a specific company. The fan is directly driven by a motor through a coupling. The main design parameters are as follows: fan rotational speed (ω) of 2850 r/min; number of impeller blades (Z) is 29; minimum distance between the impeller and volute tongue (β) is 5.5 mm; volute height (h) is 120 mm; radius of the volute tongue corner (r) is 5 mm; outlet expansion angle (θ) is 0°; and outlet length (L) is 135 mm. Figure 2 presents the 3D model of the fan, while Fig. 3 illustrates its main design parameters.

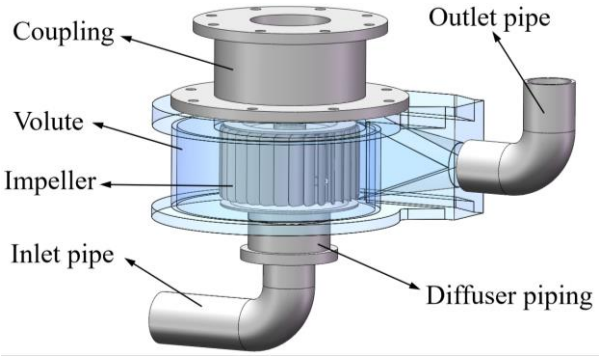

Fig. 2 Centrifugal fan 3D model

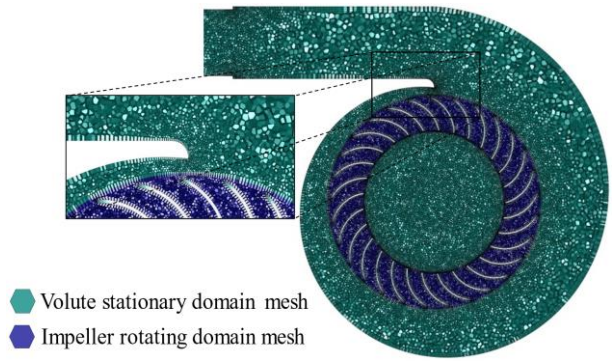

Fig. 5 Mesh generation

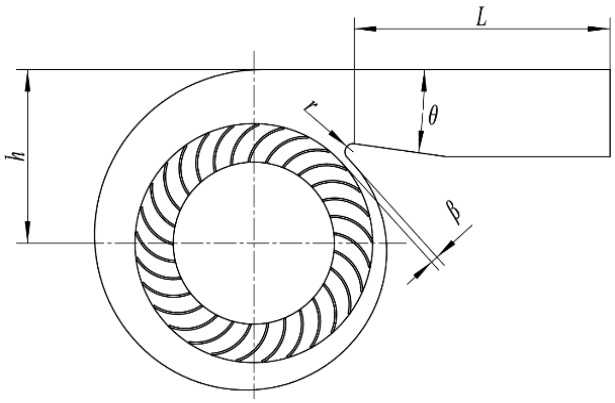

Fig. 3 Main design parameter diagram of volute

To ensure the accuracy and reliability of the numerical simulation, this study adopts a non-simplified simulation model. Additionally, to minimize the influence of inlet and outlet recirculation on the final results (Chen et al., 2007), the fan's inlet and outlet ducts are extended by 200 mm during the model pre-processing stage. The fan model is partitioned into distinct flow regions using ANSYS SpaceClaim. As shown in Fig. 4, the entire flow domain is divided into a rotating domain and a stationary domain. The rotating domain encompasses the entire impeller, while the remaining regions are treated as stationary.

Mesh generation for this study was carried out using Fluent Meshing. Due to the complex geometry of the fan's flow domain, and to reduce the number of elements and conserve computational resources, an unstructured meshing approach was adopted. A polyhedral mesh was used, offering good numerical stability and accuracy when handling complex, unstructured geometries (Martins et al., 2018). For polyhedral meshes, skewness was maintained below 0.8 to ensure mesh quality. Additionally, in all numerical simulation models, Y^+ values were controlled between 1 and 40: smaller Y^+ values were applied to the impeller blades and the volute tongue, while larger values were assigned to planar surfaces or surfaces with small curvature. This strategy was implemented to improve simulation convergence. Figure 5 illustrates the mesh generation.

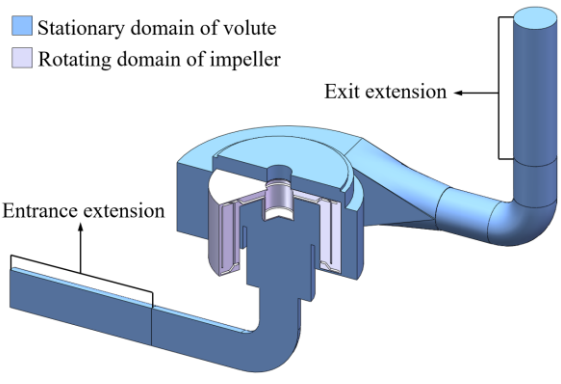

Fig. 4 Fluid domain division

2.2 Numerical Simulation Methods

Numerical simulations in this study were conducted using Fluent 2021R1. The widely used Realizable k–ε turbulence model with swirl correction (Liu, 2015) was adopted, based on a steady-state solution. The rotating domain of the impeller was defined using the Multiple Reference Frame (MRF) approach. Boundary conditions were specified as follows: the inlet was defined as a pressure inlet and the outlet as a pressure outlet, with the initial gauge pressure set to 0 Pa. The impeller blades and shaft hole wall were defined as rotating walls (Tong et al., 2020), with a rotational speed of 2850 r/min (the fan's rated speed), while all other surfaces were set as stationary walls.

The velocity–pressure coupling was solved using the SIMPLE algorithm, and all spatial discretization schemes employed the Second Order Upwind method to enhance accuracy and convergence. The simulation was set to run for 2000 iterations, with a residual convergence criterion of 1×10^{-3}. As shown in the residual plot in Fig. 6, convergence was achieved around the 1450th iteration, at which point the calculation was terminated.

To evaluate performance, the fan's Q was measured, along with the at the inlet total pressure (H_{in}) and outlet total pressure (H_{out}), from which the fan's total pressure rise (H) was calculated. The impeller shaft torque (T) was also measured to calculate the η. It is important to note that, due to the extended inlet and outlet ducts (used to mitigate recirculation effects during domain setup), validation showed pressure discrepancies across different cross-sections of the ducts. Therefore, to ensure accuracy, total pressure measurements at the inlet and outlet were taken from newly established cross-sections corresponding to the actual inlet and outlet locations.

Table 1 Mesh independence analysis table

Groups	Number of mesh elements	Outlet flow rate Q/(m^3·h^{-1})	Total pressure efficiency η/%
1	1895066	74.65	20.52
2	2190153	77.59	21.57
3	2678329	76.81	21.60
4	3022569	77.08	21.33
5	3443417	76.94	21.40
6	4230239	76.91	21.39
7	5157238	76.78	21.33

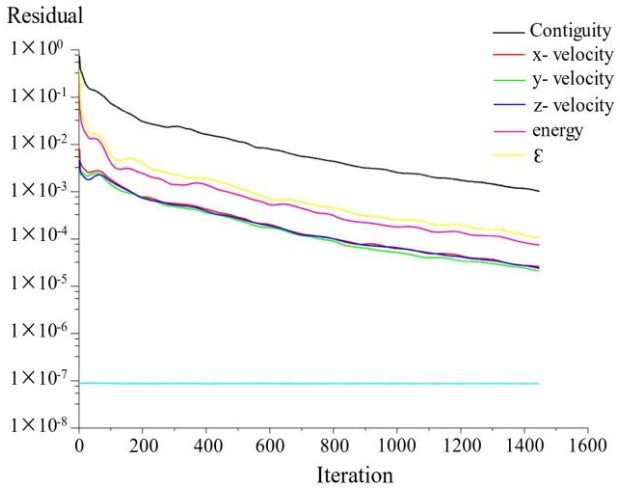

Fig. 6 Calculated residual diagram

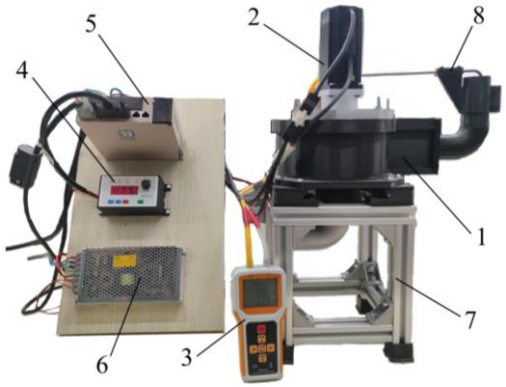

1. Centrifugal fan; 2. Drive motor; 3. Anemometer, pressure, and flow meter; 4. Speed regulator; 5. Motor driver; 6. DC power; 7. Frame; 8. L-shaped Pitot tube

Fig. 8 Experimental test platform

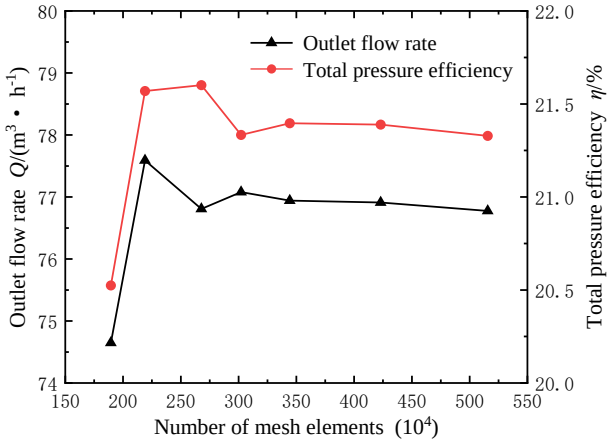

Fig. 7 Mesh independence analysis diagram

2.3 Mesh Independence Validation

To enhance computational accuracy while optimizing resource usage, a mesh independence analysis was conducted to determine the appropriate mesh size and element count. During mesh generation, parameters such as maximum mesh size, minimum mesh size, and growth rate were adjusted to control the total number of mesh elements. Seven mesh configurations were created, with element counts ranging from 1.89 million to 5.15 million, as listed in Table 1.

Numerical simulations were performed for each mesh group. As shown in Fig. 7, both the Q and η stabilized when the mesh element count exceeded 3 million.

Considering the trade-off between computational accuracy and time, Scheme 5 was selected for subsequent simulations. This scheme uses a maximum mesh size of 10 mm, a maximum mesh quality of 0.79, and a total mesh count between 3 and 4 million.

Under this mesh configuration, each numerical simulation requires approximately 4 hours to complete on a server equipped with dual 40-core CPUs (80 threads), 96 GB DDR4 memory, a GTX 1080 graphics card with 8 GB of memory, and a 960 GB SSD.

2.4 Verification of the Correctness of the Numerical Simulation

To validate the accuracy of the numerical simulation, a comparison and analysis were conducted between the simulation results and experimental data (Shen et al., 2023). The numerical simulation directly provides key performance parameters, including the Q, H_{in}, and H_{out}. Based on these, the H and T can be calculated, which are then used to determine the fan's η. The calculation formula is as follows (Arun Kumar et al., 2016):

$$H = H_{out} - H_{in} \tag{1}$$

$$\eta = \frac{\rho \cdot g \cdot Q \cdot H}{\omega \cdot T} \tag{2}$$

where ρ represents the density of the working medium, kg/m^3 while ω denotes the fan rotational speed, r/min

The experimental setup is illustrated in Fig. 8. As the T cannot be directly measured in the experiment, the η of

Table 2 P-B experiment analysis table

Variables	Sum of squares	F-value	P-value
Minimum distance between the impeller and volute tongue β	327.40	2.48	0.1664
Volute height h	234.08	1.77	0.2314
Radius of the volute tongue corner r	152.94	1.16	0.3232
Outlet expansion angle θ	125.32	0.95	0.3676
Outlet length L	129.76	0.98	0.3599

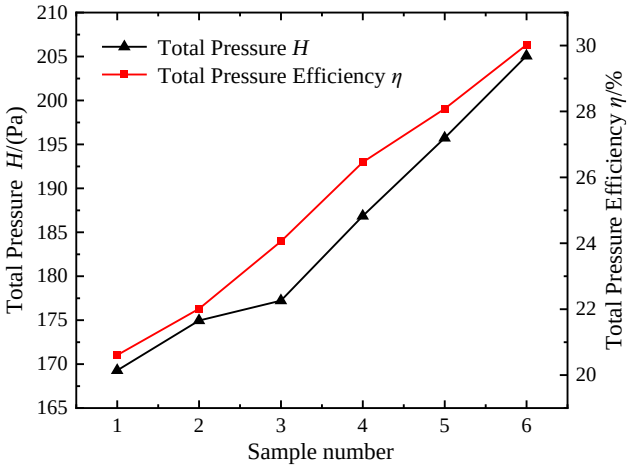

Fig. 9 Total pressure *H* and Total pressure efficiency *η* trend correlation

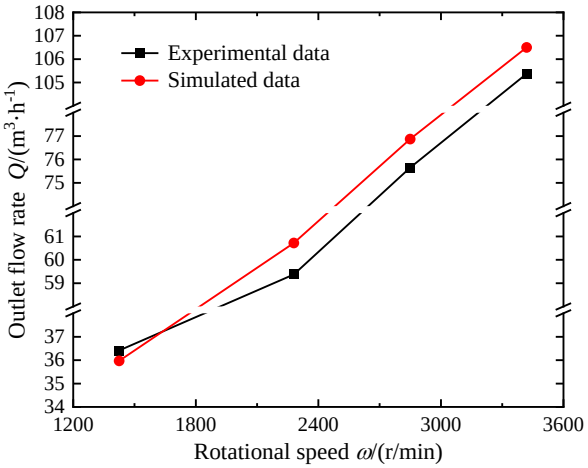

(a) Outlet flow rate *Q*

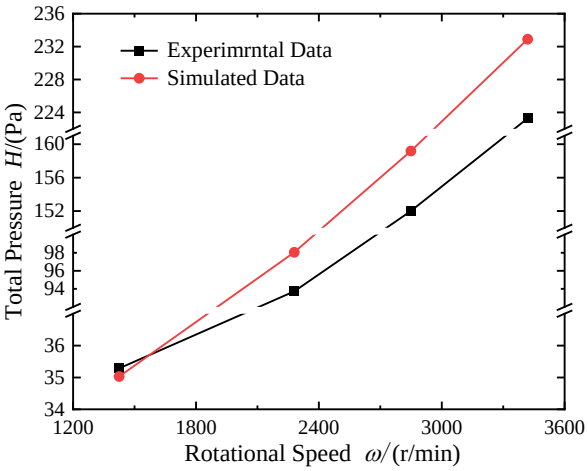

(b) Total pressure *H*

Fig. 10 Comparison of experimental and simulated data traffic

the experimental data could not be calculated. Therefore, an indirect validation was performed by analyzing the correlation between H and η across multiple samples. The results showed consistent trends between the two metrics, as presented in Fig. 9. Consequently, in subsequent experiments, performance analysis was conducted by measuring and comparing the Q and H.

These two parameters were measured using a wind speed and pressure measuring instrument at rotational speeds of 1425, 2280, 2850, and 3420 r/min. To ensure data accuracy, the L-shaped Pitot tube of the measuring instrument was positioned at seven evenly distributed points across the outlet section, and the average value was recorded. The comparison between the experimental and simulated results for the Q and H is shown in Fig. 10. The simulation results exhibit a consistent trend with the experimental data, and the deviation remains within an acceptable range, showing a maximum error of 2.3% for Q and 4.72% for H. These findings confirm the validity of the numerical simulation model and parameter settings, indicating that the model is suitable for further calculation and analysis.

3. OPTIMIZED DESIGN

3.1 Selection of Parameter Variables and Determination of Optimization Objectives

The design of a centrifugal fan volute involves multiple parameters, each exerting a different level of influence on the two target performance indicators: Q and η. Therefore, it is necessary to conduct a significance analysis of these parameters to identify the three most influential variables for use in genetic algorithm optimization.

This analysis was performed on the five primary design parameters shown in Fig. 3: β, h, r, θ, and outlet length (L).

Design Expert software was employed to design and analyze a Plackett-Burman (P-B) experiment. A total of 12 experimental groups were generated based on the five selected parameters, and numerical simulations were conducted for each group to evaluate the significance of their impact. The results, shown in Table 2, indicate that smaller p-values correspond to greater significance in influencing the target outputs, Q and η. Based on these results, the three most significant parameters were selected as optimization variables: β; h; and r. The value ranges for these parameters are defined as follows: β (mm): [4, 12]; h (mm): [115, 135]; and r (mm): [2.5, 12.5].

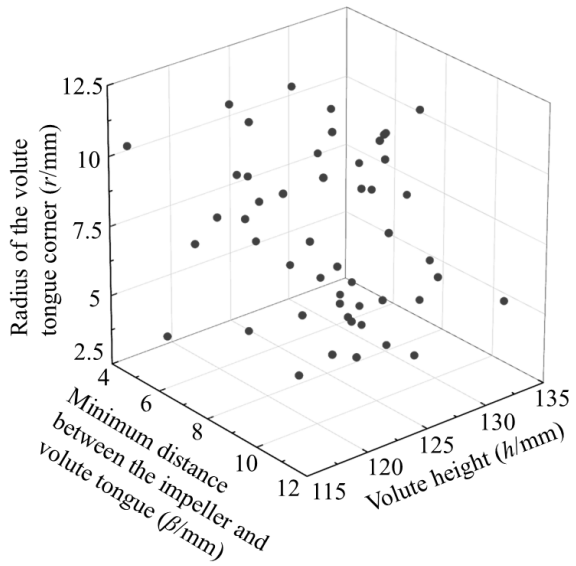

Fig. 11 Spatial distribution of variable samples

3.2 Establishment of the Sample Database

To develop an accurate and reliable neural network surrogate model, it is essential to construct a well-structured sample database for model training and prediction. By analyzing the convergence of the sample size and considering both computational cost and the accuracy requirements of the BP neural network model, a sample size of 50 was determined to be appropriate. Fifty variable combinations were randomly selected within the defined parameter ranges using the Latin Hypercube Sampling (LHS) method, and the parameter space distribution is illustrated in Fig. 11.

Subsequently, 50 fan models were created in SolidWorks 2018, and mesh generation and numerical simulations were performed in Fluent 2021R1, following the same procedures described earlier. The simulation results for each model, including the Q and η, were compiled to establish the sample database used for training the surrogate model.

3.3 Neural Network Surrogate Model

To construct a reliable surrogate model for algorithmic optimization, it is essential to accurately establish the relationship between the three design parameters (β, h, r) and the two optimization objectives (Q, η). The quality of this surrogate model directly influences the reliability of the optimization results. Given its strong nonlinear modeling capability, broad applicability, and robust learning ability (Zhang et al., 2022), the BP neural network is employed in this study to model the nonlinear relationships between the input parameters and the optimization objectives.

The BP neural network in this study is configured as follows: (1) 3 nodes in the input layer, 2 nodes in the output layer, and 10 nodes in the hidden layer, with the Tanh function as the activation function; (2) a learning rate of 0.01, a training epoch of 4000 iterations, and 10-fold cross-validation applied to the 50-sample dataset.

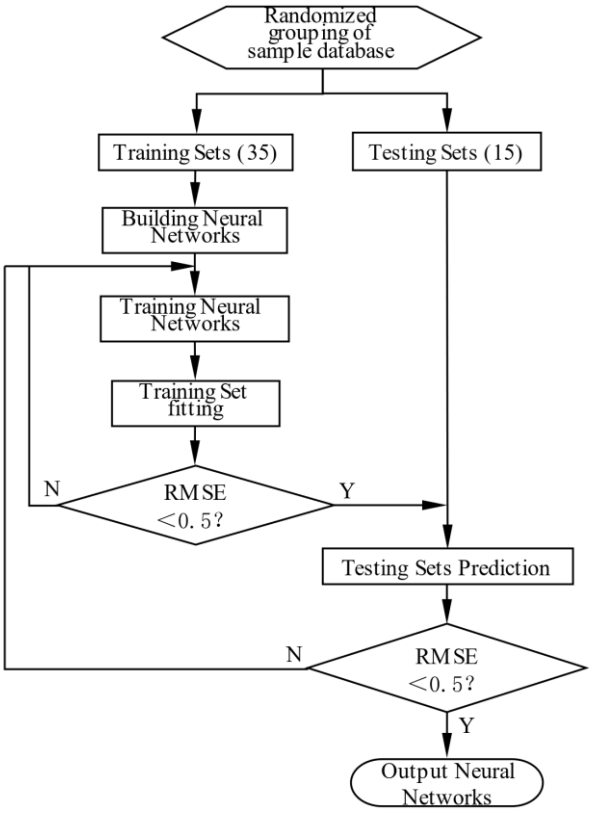

Fig. 12 BP neural network flow chart

Figure 12 illustrates the process of building the BP neural network surrogate model. The sample database, constructed as described in the previous section, is randomly divided into 35 training samples and 15 testing samples in a 7:3 ratio. The training set is used to train the neural network, while the test set is used to validate its performance. The model is considered accurate when the root mean square errors (RMSE) of both the fitting and prediction results is less than 0.5 (Tong et al., 2020). To minimize the risk of overfitting and ensure robust generalization, the cross-validation method is employed. This approach maximizes data utilization and mitigates inaccuracies caused by a limited sample size.

Figures 13 and 14 present the fitting results for the training set and the prediction results for the testing set of the BP neural network, respectively. The RMSE for the fitting and prediction of both Q and η are listed in Table 3, all of which are below 0.5. These results indicate that the BP neural network surrogate model has high accuracy and is suitable for use in the subsequent optimization process using the NSGA-III algorithm.

Table 3 Root mean square error (RMSE)

Optimization objectives		RMSE
Training sets	Outlet flow rate Q	0.23420
	Total pressure efficiency	0.31974
Testing sets	Outlet flow rate Q	0.26573
	Total pressure efficiency	0.35726

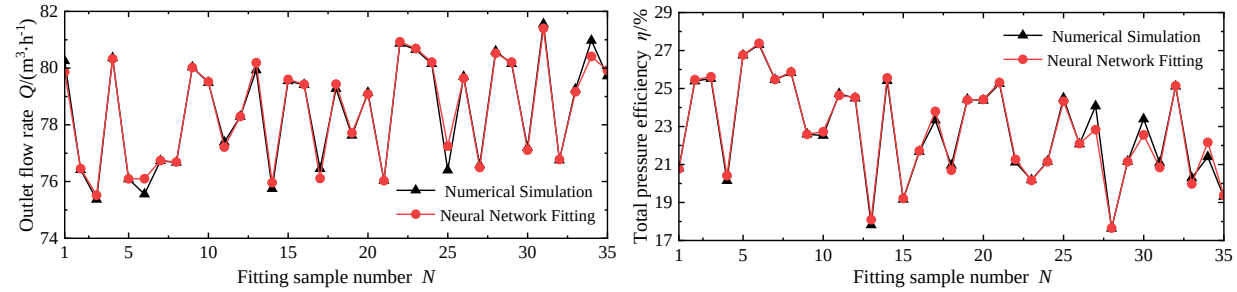

(a) (b)

Fig. 13 Training set fitting effect diagram

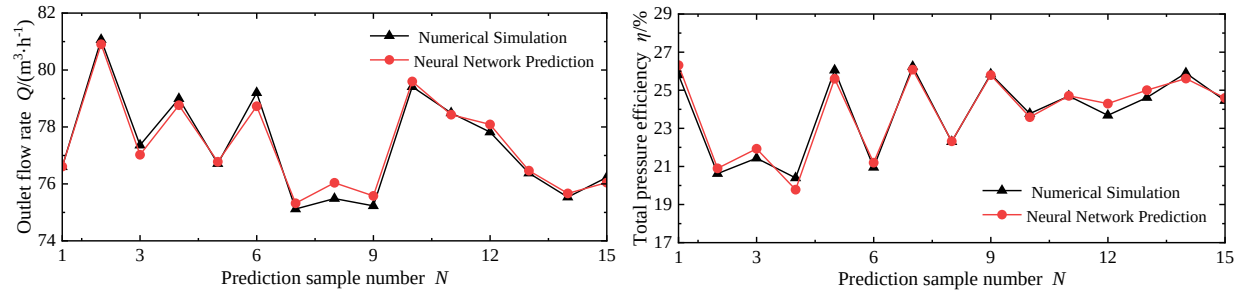

(a) (b)

Fig. 14 Test set predictive effect diagram

3.4 Genetic Algorithm Optimization

Intelligent optimization algorithms are widely applied in multi-objective design optimization. Among them, the Ant Colony Optimization (ACO), Particle Swarm Optimization (PSO), and Genetic Algorithm (GA) are the most commonly used. In this study, the Non-dominated Sorting Genetic Algorithm III (NSGA-III) is employed to perform the optimization task (Bi & Wang, 2019). This algorithm simulates the biological evolution process through mechanisms such as natural selection, inheritance, and mutation to explore optimal or near-optimal solutions within the solution space. As an enhanced version of NSGA-II, NSGA-III retains its core principles while incorporating additional features that make it more effective for high-dimensional and complex multi-objective problems. It utilizes a hierarchical decomposition approach and introduces a reference point mechanism, which improves Pareto front coverage, uniformity, and convergence (Bao et al., 2020). Compared with NSGA-II and MOEA/D algorithms, NSGA-III achieves a more uniform distribution of the solution set across the objective space, accelerates convergence, and maintains better diversity by avoiding solution clustering (Deb & Jain, 2014).

In this study, the NSGA-III algorithm is applied using the previously constructed BP neural network as the surrogate model. The optimization objectives are to maximize both the Q and η. The mathematical formulation of this multi-objective optimization problem is shown below (Tong et al., 2020):

$$\begin{cases} f_1 = Q(x)_{\max} \\ f_2 = \eta(x)_{\max} \\ x = \{\beta, h, r\}; \beta \in [4\text{mm}, 12\text{mm}] \\ h \in [115\text{mm}, 135\text{mm}]; r \in [2.5\text{mm}, 12.5\text{mm}] \end{cases} \tag{3}$$

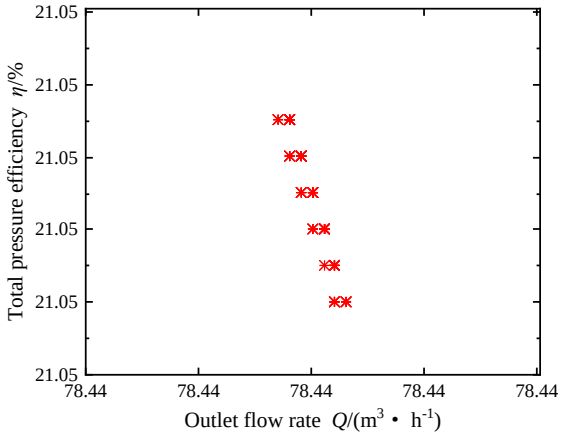

Fig. 15 Pareto optimal solution set

The specific parameter settings for the NSGA-III algorithm are as follows: the number of reference points is set to 200 to adequately cover the entire Pareto front; the population size is set to 100, which helps maintain diversity and ensures a broader exploration of the solution space, thereby reducing the risk of converging to local optima (Deb et al., 2022); and the maximum number of iterations is limited to 200 to balance computational cost with optimization performance.

Through the optimization process, the Pareto optimal solution set for the two objectives, Q and η, as well as the corresponding optimal combinations of the three design parameters were obtained, as shown in Figs. 15 and 16. These figures also illustrate the convergence trends of the objective functions and parameter variables, confirming good convergence behavior. Among the 100 non-dominated optimal solutions, the best results for Q and η are 78.44 m³/h and 21.05%, respectively. The corresponding optimal design parameters are: β = 4.57 mm, h = 116.56 mm, and r = 11.55 mm.

Table 4 Comparison of optimization results

Structures	The distance between the volute tongue and the impeller β/mm	Volute height h/mm	The radius of the volute tongue corner r/mm	Outlet flow rate (Optimization) Q/($m^3 \cdot h^{-1}$)	Total pressure efficiency (Optimization) η/%	Outlet flow rate (Simulation) Q/(m3·h^{-1})	Total pressure efficiency (Simulation) η/%
Original structure	5.50	120.00	5.00			77.08	21.77
Optimized structure	4.57	116.56	11.55	78.44	21.05	78.84	24.73

Table 5 Comparison of results under different rotational speeds

Objectives	Structures	Rotational speed ω/(r/min)			
		1425	2280	2850	3420
Outlet flow rate Q/($m^3 \cdot h^{-1}$)	Original structure	35.97	60.72	77.08	106.50
	Optimized structure	37.41	61.99	78.84	109.28
	Incremental	4.01%	2.09%	2.29%	2.61%
Total pressure efficiency η/%	Original structure	22.15	20.70	21.77	25.08
	Optimized structure	22.35	24.13	24.73	28.23
	Incremental	0.21%	3.43%	2.96	3.15%

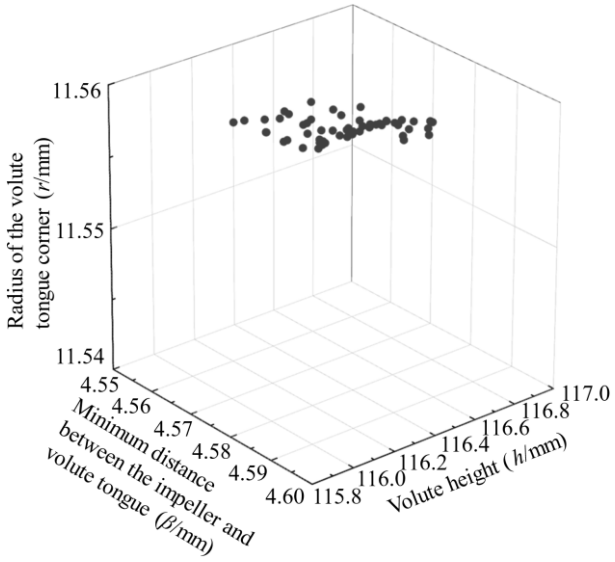

Fig. 16 Optimal combination spatial distribution of variables

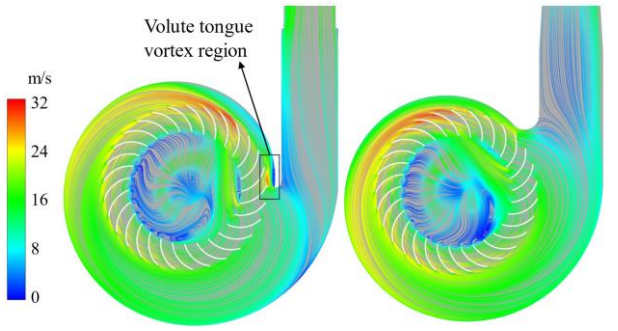

(a) Original structure (b) Optimized structure

Fig. 17 Radial center plane streamline distribution

4. OPTIMIZATION RESULTS ANALYSIS

4.1 Verification of Optimization Results

To verify the accuracy of the optimization results, a 3D model was created based on the optimal combination of design variables, and numerical simulations were conducted. Table 4 presents a comparison between the predicted algorithmic results and the simulation results for Q and η. The errors between the numerical simulation and the optimized predictions are 0.51% for Q and 3.68% for η, indicating that the optimization results are reliable. Moreover, when comparing the optimized structure to the original design, the Q increased by 2.29%, and the η improved by 2.96%, demonstrating significant improvements in both optimization objectives.

The results discussed above were obtained at the rated speed (ω) of 2850 r/min. To assess the performance of the optimized design under varying operating conditions, numerical simulations were conducted at three additional common speeds. The comparison of Q and η at these speeds with the original structure is shown in Table 5. As seen in the table, at speeds ω_1: 1425 r/min, ω_2: 2280 r/min, ω_3: 2850 r/min, and ω_4: 3420 r/min, the optimized structure shows increases in Q of 4.01%, 2.09%, 2.29%, and 2.61%, respectively, and increases in η of 0.21%, 3.43%, 2.96%, and 3.15%, respectively, compared to the original structure. Both Q and η exhibit significant improvements. Additionally, it is observed that both outlet flow rate and total pressure efficiency increase gradually as the rotational speed rises. The fluctuations in performance improvements with rotational speed can be attributed to the influence of the Reynolds number effect and boundary layer behavior.

4.2 Internal Flow Field Analysis

Figure 17 presents a comparison of the radial central plane flow fields for the fans of the original and optimized

Table 6 Comparison of improved structure results

Structures	Outlet flow rate Q/($m^3 \cdot h^{-1}$)	Incremental	Total pressure efficiency η/%	Incremental
Original structure	77.08		21.77	
Optimized	78.84	2.29%	24.73	2.96%
Improved structure	81.75	6.06%	26.17	4.40%

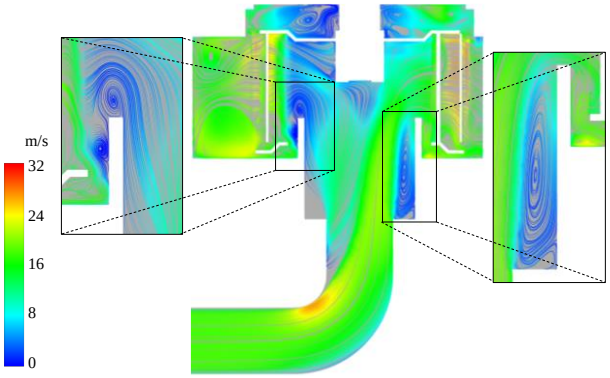

(a) Optimized structure

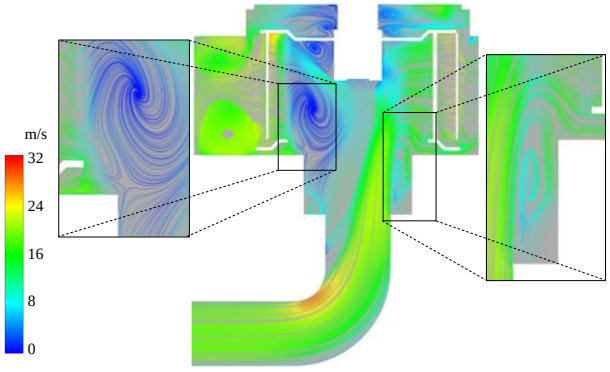

(b) Improved structure

Fig. 18 Axial center plane streamline distribution

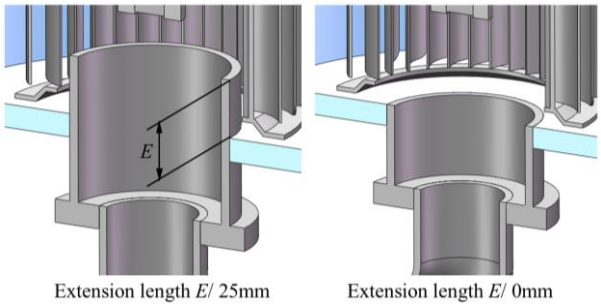

(a) Optimized structure (b) Improved structure

Fig. 19 Inlet structures improvement diagram

structures. In the original design, the gas predominantly flows along the inner side of the outlet pipe, with a significant portion of the gas recirculating at the volute tongue, forming a vortex region. In contrast, the optimized structure exhibits gas flowing primarily along the outer side of the outlet pipe, eliminating the vortex phenomenon at the volute tongue. This suggests that the flow field within the optimized fan is improved, leading to an increase in the Q, which subsequently enhances the fan's η.

Further analysis of the axial center plane flow field distribution for the optimized structure, shown in Fig. 18a, reveals that in the gas inlet diffusion area, the pipeline extends above the volute bottom surface by an extension length (E), as shown in Fig. 19a. This extension causes vortex regions to form around the inlet, resulting in turbulent gas flow in nearby areas and impacting the overall internal flow field. To address this, an attempt was made to shorten the E of the pipeline at the inlet, aligning it flush with the volute bottom surface, as illustrated in Fig. 19b. Following numerical simulations, Fig. 18b illustrates the internal flow field of the improved structure, where the vortex phenomenon around the inlet is reduced, resulting in a smoother overall flow field compared to the previous design. Table 6 provides a comparison of the Q and η for the improved structure, original structure, and optimized structure at the ω of 2850 r/min.

At the ω of 2850 r/min, shortening the E to align with the volute bottom surface in the improved structure resulted in a 6.06% increase in Q and a 4.40% increase in η compared to the original structure. In comparison to the optimized structure, Q increased by 3.77% and η by 1.44%. These results demonstrate the effectiveness of the structural improvements in this area.

4.3 Experimental Verification

To verify the correctness and effectiveness of the improvements, experimental tests were conducted on both the optimized and improved structures, followed by a comparative analysis. The experimental platform used was the same as described in Section 2.4. Due to

experimental constraints, the T could not be directly measured, and therefore, the η could not be calculated. Instead, an SG-312 type anemometer (Fig. 20a) was used to measure the Q and H of the fan. To ensure accurate measurements, the fan outlet was extended by 50mm, and the L-shaped Pitot tube was inserted at the outlet to measure the section at the same height as the numerical simulation monitoring position. Figure 20b shows the seven measurement points arranged uniformly on the outlet cross-section, with the average of the data taken for analysis.

The experimental measurement data for the Q and H of the optimized and improved structures at various speeds are shown in Table 7. A comparison between the optimized structure (obtained through parameter optimization using the NSGA-III algorithm) and the original structure at the rated speed of 2850 r/min reveals an outlet flow rate of 76.81 m^3/h (a 3.13% increase) and a total pressure of 161.14 Pa (a 6.02% increase). Additionally, at other speeds, both Q and H showed improvements. For the improved structure, which included

Table 7 Optimize and improve the structural experimental data

Rotational speed ω/(r/min)	Original structure		Optimized structure				Improved structure			
	Outlet flow rate Q/(m^3·h^{-1})	Total pressure H/(Pa)	Outlet flow rate Q/(m^3·h^{-1})	Incremental	Total pressure H/(Pa)	Incremental	Outlet flow rate Q/(m^3·h^{-1})	Incremental	Total pressure H/(Pa)	Incremental
1425	36.41	35.29	37.08	1.83%	36.57	3.64%	37.62	3.30%	38.00	7.69%
2280	59.37	93.71	60.80	2.41%	98.43	5.03%	62.66	5.54%	104.43	11.43%
2850	75.65	152.00	76.81	3.13%	161.14	6.02%	79.93	5.65%	167.86	10.43%
3420	105.37	223.29	107.04	2.93%	242.86	8.77%	112.21	6.49%	252.00	12.86%

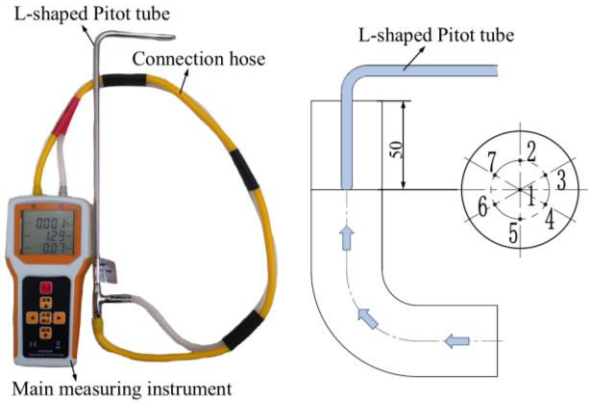

(a) SG-312 flow rate and pressure measuring instrument

(b) Schematic layout of measurement points on the cross-section

Fig. 20 Experimental measurement instruments and layout diagram

modifications to the inlet diffuser pipe after analyzing the internal flow field, the performance at the rated speed was enhanced, with an outlet flow rate of 79.93 m^3/h (a 5.56% increase) and a total pressure of 167.86 Pa (a 10.43% increase). At multiple speeds, improvements over both the original and optimized structures were significant. At a speed of 3420 r/min, the outlet flow rate reached 112.21 m^3/h, and the total pressure was 252 Pa, marking the largest increases of 6.49% and 12.86%, respectively. Data analysis reveals that both the optimized and improved structures show a consistent trend of increasing Q and H, as the speed increases, compared to the original structure.

The experimental measurement data and numerical simulation results are in good agreement, both in magnitude and trend, with the maximum error being 3%. This further confirms the accuracy of the numerical simulation model. Moreover, the increases in Q and H are consistent with the optimization and simulation results, verifying the effectiveness of the optimization and improvements.

5. CONCLUSION

This study focuses on optimizing the centrifugal fan design by using the Q and η as objectives, with β, h, and r as the optimization variables. The multi-objective optimization is performed using the NSGA-III algorithm based on a BP neural network surrogate model. The main conclusions are as follows: First, a mesh independence analysis identified that the mesh size should be between 3 million and 4 million cells. The simulation accuracy was verified through experiments, confirming high accuracy and correct simulation settings, including the turbulence model and pressure-velocity coupling method. Second, a Plackett-Burman experiment was used to analyze the impact of five key volute design parameters on Q and η. The parameters were ranked in the following order of influence: β, h, r, θ, and L. The first three parameters were selected for optimization. Third, the BP neural network surrogate model, trained with fifty samples generated by Latin Hypercube Sampling, achieved RMSE of 0.26573 for Q and 0.35726 for η. This demonstrates the model's strong predictive accuracy for centrifugal fan performance. Fourth, the NSGA-III algorithm optimized the design, producing a Pareto optimal solution set with good convergence. The optimal solutions for Q and η were 78.44 m^3/h and 21.05%, respectively, with the corresponding optimal parameters: r = 4.57 mm, β = 4.57 mm, and h = 116.56 mm. Numerical simulations showed improvements in both Q and η for the optimized structure, with the disappearance of vortices at the volute tongue and a reduction in inlet vortex phenomena through structural modification. Sixth, experimental tests on the optimized and improved structures confirmed the simulation results. The optimized structure achieved a 3.13% increase in Q and a 6.02% increase in H. After improving the inlet structure, the outlet flow rate increased by 5.56%, and total pressure by 10.43%. At a speed of 3420 r/min, the increases reached 6.49% and 12.86%, respectively. Both the optimized and improved structures showed enhanced performance compared to the original structure as speed increased. Finally, this study proposes a comprehensive method for optimizing centrifugal fan volute parameters using a BP neural network surrogate model and the NSGA-III algorithm, achieving a 6.06% increase in Q and a 4.04% improvement in η. The integration of numerical simulation, experimental validation, and structural improvement represents a robust methodology, with the structural modification of the inlet duct to minimize vortices offering valuable practical insights. This work fills a gap in the literature and advances both research and engineering applications in centrifugal fan design.

FUNDING

The author(s) disclosed receipt of the following financial support for the research, authorship, and/or publication of this article: The authors gratefully

acknowledge the support of the National Natural Science Foundation of China (Grant No.52165013, No.51565021) for this study.

CONFLICT OF INTEREST

The authors declare that they have no known competing financial interests or personal relationships that could have appeared to influence the work reported in this paper.

AUTHORS CONTRIBUTION

J. L. Li: Conceptualization, Data curation, Investigation, Methodology, Software, Visualization, Formal analysis, Writing original draft. **X. J. Wang:** Conceptualization, Supervision, Methodology, Resources, Writing review & editing. **H. Gong:** Experimental equipment, Software. **J. J. Wang:** Methodology, Supervision, Writing review & editing.

REFERENCES

Ai, W. S., & Chen, X. J. (2016). Influence of inlet angle of blades on noise from multi-blade centrifugal fans. *Chinese Journal of Turbomachinery*, (02), 37-41. https://doi.org/10.16492/j.fjjs.2016.02.0112

Amiet, R. K. (1976). Noise due to turbulent flow past a trailing edge, *Journal of Sound and Vibration*, *47* (3), 387-393. https://doi.org/10.1016/0022-460X(76)90948-2

Arun kumar, P., Senthil, P., & Naveen kumar, K. (2016). Analysing mass flow rate and noise level of blowers through Ansys CFX solver. *Australian Journal of Mechanical Engineering*, *15*(3), 175–181. https://doi.org/10.1080/14484846.2016.1230311

Bao, Z. Y., Yu, J. Z., & Yang, S. (2020) *Intelligent optimization algorithms and MATLAB examples*. Beijing: Publishing House of Electronics Industry.

Bi, X. J., & Wang, C. (2019). A reference point constrained dominance-based NSGA-II algorithm. *Control and Decision*, *34*(2), 369-376. https://doi.org/10.13195/j.kzyjc.2017.1067

Chen, C. H., Yang, Q., & Cheng, Y. (2019). Numerical study of the effect of lobe-top spacing of the worm tongue on the aerodynamic noise of centrifugal fans. *Technology and Market*, *25*(11), 46-47. https://doi.org/10.3969/j.issn.1006-8554.2018.11.017

Chen, S. Y., Sui, X., & Wang, C. X. (2007). Three-dimensional Numerical Simulation of the Internal Flow in the Centrifugal Fan. *Fluid Machinery*, *35*(9), 22-25. https://doi.org/10.3969/j.issn.1005-0329.2007.09.006

Deb, K., & Jain, H. (2014). An evolutionary many-objective optimization algorithm using reference-point-based nondominated sorting approach, Part I: Solving problems with box constraints. *IEEE Transactions on Evolutionary Computation*, *18*(4), 577-601. https://doi.org/10.1109/TEVC.2013.2281535.

Deb, K., Pratap, A., Agarwal, S., & Meyarivan, T. (2022). A fast and elitist multiobjective genetic algorithm: NSGA-II. *IEEE Transactions on Evolutionary Computation*, *6*(2), 182-197. https://doi.org/10.1109/4235.996017

Huang, C. H., & Tseng, W. C. (2016). An optimal volute spiral case design for centrifugal fan: theoretical and experimental studies. *International Journal of Mechanics and Materials in Design*, *12*, 223–240. https://doi.org/10.1007/s10999-015-9303-4

Li, Y., Zhao, C., Lu, F. A., & Ren, G. (2012). Numerical optimization on the volute configuration of a centrifugal fan via variable helical angle. *Chinese Journal of Applied Mechanics*, *29*(4), 398-403. https://doi.org/10.11776/cjam.29.04.A036

Li, Z. H., & Zheng X. Q. (2017). Review of design optimization methods for turbomachinery aerodynamics, *Progress in Aerospace Sciences*, *93*, 1-23. https://doi.org/10.1016/j.paerosci.2017.05.003

Liang, L., Gong, W. Q., Liu, Y. T., & Wang, F. (2023). Multi-objective optimization and performance analysis of centrifugal compressor impeller based on the immune algorithm. *Journal of Xi'an Jiaotong University*, *58*(02), 56-65. https://doi.org/10.7652/xjtuxb202402006

Liu, Z. Z. (2015). *Investigation on plate heat transfer and resistance characteristies and stamping process of plate heat exchangers*. Jinan, Shandong University.

Ma, N., Meng, J., Luo, J., & Liu, Q. (2024). Optimization of thermal-fluid-structure coupling for variable-span inflatable wings considering case correlation. *Aerospace Science and Technology*, *153*, 109448. https://doi.org/10.1016/j.ast.2024.109448.

Martins, D. M., Albuquerque, D. M., & Pereira, J. C. (2018). On the use of polyhedral unstructured grids with a moving immersed boundary method. *Computers & Fluids*, *174*, 78-88. https://doi.org/10.1016/j.compfluid.2018.07.010

Patil, S. R., Chavan, S. T., Jadhav, N. S., & Vadgeri, S. S. (2018). Effect of volute tongue clearance variation on performance of centrifugal blower by numerical and experimental analysis. *Materials Today: Proceedings*, *5*(2), 3883-3894. https://doi.org/10.1016/j.matpr.2017.11.643

Shen, Y., Lu, Q., & Li, Y. (2023). Design criterion and analysis of hybrid-excited vernier reluctance linear machine with slot halbach PM arrays. *IEEE Transactions on Industrial Electronics*, *70*(5), 5074-5084, https://doi.org/10.1109/TIE.2022.3183278.

Shinbara, N., Hatakeyama, M., Kodama, Y., & Hayashi, H. (1996). Characteristics of fluid dynamics and noise of a multiblade radial fan. Effects of inner diameter and the number of blades on the characteristics of fluid dynamics and noise. *Nippon Kikai Gakkai Ronbunshu. B Hen (Transactions of*

the Japan Society of Mechanical Engineers. Part B), *62*, 110-116.

Tantakitti, P., Pattana, S., & Wiratkasem, K. (2018). *The performance of backward curved centrifugal fan with various impeller inlet and outlet angles.* 2018 Third International Conference on Engineering Science and Innovative Technology (ESIT), (pp. 1-3). https://doi.org/10.1109/ESIT.2018.8665280

Tao, Z., Li, W., Guo, Z., Chen, Y., Song, L., & Li, J. (2024). Aerothermal optimization of a turbine rotor tip configuration based on free-form deformation approach. *International Journal of Heat and Fluid Flow*, *110*, 109644. https://doi.org/10.1016/j.ijheatfluidflow.2024.109644.

Tong, M. Z., Chen, X., Tong, S. G., Yu, Y., Li, J. F., & Hao, G. S. (2020). Multi-objective optimization design of low specific speed centrifugal pumps based on NSGA-III algorith. *China Mechanical Engineering*, *31*(18), 2239-2246. https://doi.org/10.3969/j.issn.1004-132X.2020.18.012

Wang, C. L., Hu, B. B., Feng Y. M., & Liu, K. K. (2019). Multi-objective optimization of double vane pump based on radial basis neural network and particle swarm. *Transactions of the Chinese Society of Agricultural Engineering (Transactions of the CSAE)*, *35*(2), 25 — 32. https://doi.org/10.11975/j.issn.1002-6819.2019.02.004

Wu, Y., Dou, H. S., Wei, Y. K., Chen, X. P., Chen, Y. N., & Cao, W. B. (2002). *Effect of attack angle on flow characteristic of centrifugal fan.* IOP Conference Series: Materials Science and Engineering. 129(1), 012-059. https://doi.org/10.1088/1757-899X/129/1/012059

Zhang, D. S., Yang, G., Zhao, X. T., Yang, X, Q., & Gao, X. F. (2022). Optimization design of vane diffuser and volute in vertical centrifugal pump based on back propagation neural network. *Transactions of the Chinese Society of Agricultural Engineering (Transactions of the CSAE)*, *53*(04), 130-139. https://doi.org/10.6041/j.issn.1000-1298.2022.04.013

Zhang, X., Zhu, Q., Wang, S., Ma, T., Gao, S., Kong, Y., Han, Q., & Chu, F., (2025). Hybrid triboelectric-variable reluctance generator assisted wireless intelligent condition monitoring of aero-engine main bearings. *Nano Energy*, *136*, 110721. https://doi.org/10.1016/j.nanoen.2025.110721.

Zhang, Z. J., Yu, Q. Y., Deng, Y. L., & Wu, P. (2023). Multi-factor orthogonal experimental optimization design of an industrial fan considering the clearance between impeller and casing. *Fluid Machinery*, *51*(06), 26-32. https://doi.org/10.3969/j.issn.1005-0329.2023.06.005

Zhao, T., Zhao, C., Ren, G., & Shi, T. Q. (2012). Experimental study on the effect of inclined volute tongue on the noise reduction of centrifugal fan. *Fluid Machinery*, (03), 1-7. https://doi.org/10.3969/j.issn.1005-0329.2012.03.001

Zhou, S. Q., Dong, H. B., Zhang, K., Zhou, H. X., Jin, W. Y. & Wang, C. H. (2021). Optimal design of multi-blade centrifugal fan based on partial coherence analysis. *Journal of Mechanical Engineering Science*, *236*(2), 894-907. https://doi.org/10.1177/0954406221999683

Zhou, S. Q., Wang, M., Li, Z. Y., & Zhang, S. C. (2018). Influence of volute retrofit design on performance of multi-blade centrifugal fan. *Transactions of the Chinese Society for Agricultural Machinery*, *49*(10), 180-186+249. https://doi.org/10.6041/j.issn.1000-1298.2018.10.020

Zuo, S. G., Wei, K. J., Wu, X. D., Nie, Y. J., & Xu, S. C. (2016). Multi-objective parameter optimization of centrifugal compressor impeller with Kriging model. *Transactions of the Chinese Society of Agricultural Engineering (Transactions of the CSAE)*, *32*(2), 77-83. https://doi.org/10.11975/j.issn.1002-6819.2016.02.012